Submitted to

XV International Workshop on Deep-Inelastic Scattering and Related Subjects,
DIS 2007 April 16-20, 2007, Munich

www-h1.desy.de/h1/www/publications/conf/conf_list.html

A general search for new phenomena at HERA

H1 Collaboration

Abstract

A model-independent search for deviations from the Standard Model prediction is performed in e^+p and e^-p collisions at HERA II using all H1 data recorded during this second running phase. This corresponds to integrated luminosities of 178 pb^{-1} and 159 pb^{-1} for e^+p and e^-p collisions, respectively. All event topologies involving isolated electrons, photons, muons, neutrinos and jets with high transverse momenta are investigated in a single analysis. Events are assigned to exclusive classes according to their final state. A statistical algorithm is used to search for deviations from the Standard Model in the distributions of the scalar sum of transverse momenta or invariant mass of final state particles and to quantify their significance. A good agreement with the Standard Model prediction is observed in most of the event classes. No significant deviation is observed in the phase-space and in the event topologies covered by this analysis.

1 Introduction

At HERA electrons[1] and protons collide at a centre-of-mass energy of up to 319 GeV. These high-energy electron-proton interactions provide a testing ground for the Standard Model (SM) complementary to e^+e^- and $p\bar{p}$ scattering.

The approach described in this paper consists of a comprehensive and generic search for deviations from the SM prediction at large transverse momenta. The present analysis follows closely the strategy of our previous publication [1]. All high P_T final state configurations involving electrons (e), muons (μ), jets (j), photons (γ) or neutrinos (ν) are systematically investigated. The analysis covers phase space regions where the SM prediction is sufficiently precise to detect anomalies and does not rely on assumptions concerning the characteristics of any SM extension.

All final states containing at least two objects (e, μ, j, γ, ν) with $P_T > 20$ GeV in the polar angle[2] range $10° < \theta < 140°$ are investigated. The complete HERA II data sample (2003–2007) is used, corresponding to a total integrated luminosity of 337 pb^{-1} shared between e^+p (178 pb^{-1}) and e^-p (159 pb^{-1}) collisions. All selected events are classified into exclusive event classes according to the number and types of objects detected in the final state (e.g. e-j, μ-j-ν, j-j-j-j-j). These exclusive event classes ensure a clear separation of final states and allow an unambiguous statistical interpretation of deviations. All experimentally accessible combinations of objects have been studied and data events are found in 23 of them.

In a first analysis step the global event yields of the event classes are compared with the SM expectation. The distributions of the invariant mass M_{all} and of the scalar sum of transverse momenta $\sum P_T$ of high P_T final state objects are presented. New physics may be visible as an excess or a deficit in one of these distributions. Therefore, in a second step these distributions are systematically investigated using a dedicated algorithm which locates the region with the largest deviation of the data from the SM prediction. The probability of occurrence of such a deviation is derived, both for each event class individually and globally for all classes combined.

2 Standard Model processes and Monte Carlo generation

Several Monte Carlo event generators are combined to simulate events for all dominant SM processes, avoiding double-counting. All processes are generated with an integrated luminosity significantly higher than that of the data sample and events are passed through a full detector simulation [2]. At high transverse momenta the dominant SM processes are the photoproduction of two jets and neutral current (NC) deep-inelastic scattering (DIS). In the following the abbreviation X represents the reaction products not belonging to the high P_T objects considered.

[1] In this paper "electrons" refers to both electrons and positrons, if not otherwise stated.

[2] The origin of the H1 coordinate system is the nominal ep interaction point, with the direction of the proton beam defining the positive z-axis (forward region). The transverse momenta are measured in the xy plane. The pseudorapidity η is related to the polar angle θ by $\eta = -\ln\tan(\theta/2)$.

Photoproduction of jets and photons To simulate the direct and resolved photoproduction of jets $ep \to jjX$, prompt photon production $ep \to \gamma jX$ and the resolved photoproduction of photon pairs $ep \to \gamma\gamma X$, the PYTHIA 6.1 event generator [3] is used. Light and heavy flavoured jets are generated. The simulation contains the Born level hard scattering matrix elements and radiative QED corrections.

Neutral current deep-inelastic scattering The Born, QCD Compton and Boson Gluon Fusion matrix elements are used in the RAPGAP [4] event generator to model NC DIS events. The QED radiative effects arising from real photon emission from both the incoming and outgoing electrons are simulated using the HERACLES [5] generator. Hence the NC DIS prediction contains the processes $ep \to ejX$, $ep \to ejjX$ and $ep \to e\gamma jX$. If the electron has $P_T < 20$ GeV, NC DIS may contribute to the $ep \to jjX$ and $ep \to \gamma jX$ processes.

Charged current deep-inelastic scattering Charged current (CC) DIS events are also simulated using the RAPGAP [4] program. This prediction contributes to the final states $ep \to \nu jX$, $ep \to \nu jjX$ and to final states with an additional radiated photon.

QED Compton scattering Elastic and quasi-elastic Compton processes $ep \to e\gamma X$ are simulated with the WABGEN [6] generator. The inelastic contribution is already included in the NC DIS RAPGAP sample.

Electroweak production of lepton pairs Multi-lepton events (ee, $\mu\mu$, $\tau\tau$) are generated with the GRAPE [7] program, which includes all electroweak matrix elements at tree level. Multi-lepton production via $\gamma\gamma$, γZ, ZZ collisions, internal photon conversion and the decay of virtual or real Z bosons is considered. Initial and final state QED radiation is included. The complete hadronic final state is obtained via interfaces to PYTHIA and SOPHIA [8] for the inelastic and quasi-elastic regimes, respectively. Consequently, GRAPE predicts $ep \to \mu\mu X$ and $ep \to eeX$, as well as $ep \to e\mu\mu X$ and $ep \to eeeX$ if the scattered electron is detected. Processes with an additional radiated photon are also modelled.

W production The production of W bosons $ep \to WX$ and $ep \to WjX$ is modelled using EPVEC [9]. Next-to-leading order QCD corrections [10] are taken into account by reweighting the events as a function of the transverse momentum and rapidity of the W boson [11].

Processes with the production of three or more jets, e.g. $ep \to jjjX$ or $ep \to jjjjX$, are accounted for using leading logarithmic parton showers as a representation of higher order QCD radiation. Hadronisation is modelled using Lund string fragmentation [3]. The prediction of processes with two or more high transverse momentum jets, e.g. $ep \to jjX$, $ep \to ejjX$ is scaled by a factor of 1.2 to normalise the leading order Monte Carlos to next-to-leading order QCD calculations [12].

3 Experimental technique

3.1 The H1 detector

The H1 detector [14] components relevant to the present analysis are briefly described here. Jets, photons and electrons are measured with the Liquid Argon (LAr) calorimeter [15], which covers the polar angle range $4^\circ < \theta < 154^\circ$ with full azimuthal acceptance. Electromagnetic shower energies are measured with a precision of $\sigma(E)/E = 12\%/\sqrt{E/\mathrm{GeV}} \oplus 1\%$ and hadronic energies with $\sigma(E)/E = 50\%/\sqrt{E/\mathrm{GeV}} \oplus 2\%$, as measured in test beams. The central and forward tracking detectors are used to measure charged particle trajectories, to reconstruct the interaction vertex and to supplement the measurement of the hadronic energy. The LAr and inner tracking detectors are enclosed in a super-conducting magnetic coil with a strength of 1.15 T. The return yoke of the coil is the outermost part of the detector and is equipped with streamer tubes forming the central muon detector ($4^\circ < \theta < 171^\circ$). It is also used to supplement the measurement of hadrons. In the forward region of the detector ($3^\circ < \theta < 17^\circ$) a set of drift chamber layers (the forward muon system) detects muons and, together with an iron toroidal magnet, allows a momentum measurement. The luminosity measurement is based on the Bethe-Heitler process $ep \to ep\gamma$, where the photon is detected in a calorimeter located downstream of the interaction point.

The main trigger for events with high transverse momentum is provided by the LAr calorimeter. The trigger efficiency is close to 100% for events having an electromagnetic deposit in the LAr (electron or photon) with transverse momentum greater than 20 GeV [17]. Events triggered only by jets have a trigger efficiency close to 100% for $P_T^{jet} > 20$ GeV. For events with missing transverse momentum above 20 GeV, determined from an imbalance in the transverse momentum measured in the calorimeter, the trigger efficiency is $\sim 90\%$. The muon trigger is based on single muon signatures from the central muon detector, which are combined with signals from the central tracking detector. The trigger efficiency for di-muon events is about 70%.

3.2 Event selection

At HERA electrons or positrons with an energy of 27.6 GeV collide with protons at an energy of 920 GeV resulting in a centre-of-mass energy of $\sqrt{s}$ = 319 GeV. The event sample studied consists of the full 2003–2007 HERA II data set. It corresponds to an integrated luminosity of 337 pb^{-1} recorded in both positron–proton and electron–proton collision modes.

The data selection requires at least one isolated electromagnetic cluster, jet or muon to be found in the detector acceptance. Energy deposits in the calorimeters and tracks in the inner tracking system are combined to reconstruct the hadronic energy. To reduce background it is demanded that the event vertex be reconstructed within 35 cm in z of the nominal position and that $\sum_i (E_i - P_{z,i}) < 75$ GeV, where E_i is the particle's energy and $P_{z,i}$ is the z component of the particle momentum. Here, the index i runs over all hadronic energy deposits, electromagnetic clusters and muons found in the event. Due to energy-momentum conservation events are expected to have a value of $\sum_i (E_i - P_{z,i}) = 55.2$ GeV, twice the electron beam energy, if only longitudinal momentum along the proton beam direction is unmeasured. Events with topologies typical of cosmic ray and beam-induced background are rejected. Moreover, the timing of the event is required to coincide with that of the ep bunch crossing.

The identification criteria for each type of particle are similar to those applied in our previous general search [1]. The following paragraphs describe the identification criteria for the different objects and give the identification efficiencies for the kinematic region considered in the analysis.

Electron identification The electron identification is based on the measurement of a compact and isolated electromagnetic shower in the LAr calorimeter. The hadronic energy within a distance in the pseudorapidity-azimuth ($\eta - \phi$) plane $R = \sqrt{(\Delta\eta)^2 + (\Delta\phi)^2} < 0.75$ around the electron is required to be below 2.5% of the electron energy. This calorimetric electron identification is complemented by tracking conditions. A high quality track is required to geometrically match the electromagnetic cluster within a distance of closest approach to the cluster centre-of-gravity of 12 cm. No other good track is allowed within $R < 0.5$ around the electron direction. In the central region ($20^\circ < \theta < 140^\circ$) the distance between the first measured point in the central drift chambers and the beam axis is required to be below 30 cm in order to reject photons that convert late in the central tracker material. In addition, the transverse momentum measured from the associated track $P_T^{e_{tk}}$ is required to match the calorimetric measurement P_T^e with $1/P_T^{e_{tk}} - 1/P_T^e < 0.04$ GeV^{-1}. In the region not fully covered by the central drift chambers ($10^\circ < \theta < 37^\circ$) a wider isolation cone of $R = 1$ is required to reduce the contribution of fake electrons from hadrons. The resulting electron finding efficiency is $\sim 90\%$ in the central region and 70% in the forward region.

Photon identification The photon identification relies on the measurement of an electromagnetic shower and on the same calorimetric isolation criteria against hadrons as for the electron identification. In addition, photons are required to be separated from jets with $P_T^{jet} > 5$ GeV by a distance of $R > 1$ to the jet axis. Vetoes on any charged track pointing to the electromagnetic cluster are applied. No track with a distance of closest approach to the cluster below 24 cm should be present. The resulting photon identification efficiency as derived using elastic QED Compton events is $\sim 85\%$.

Muon identification The muon identification is based on a track in the forward muon system or in the inner tracking systems associated with a track segment or an energy deposit in the central muon detector. The muon momentum is measured from the track curvature in the toroidal or solenoidal magnetic fields. A muon candidate should have no more than 5 GeV deposited in a cylinder of radius 25 cm and 50 cm in the electromagnetic and hadronic sections of the LAr calorimeter, respectively, centred on the muon track direction. In di-muon events, the requirement of an opening angle between the two muons smaller than 165° discards events with muons coming from cosmic rays. Beam halo muons are rejected by requiring that the muons originate from the event vertex. Finally, misidentified hadrons are almost completely suppressed by requiring that the muon candidate is separated from the closest jet with $P_T > 3$ GeV by $R > 1$. The efficiency to identify muons is greater than 90%.

Jet identification Jets are defined using the inclusive $k_\perp$ algorithm [21, 22]. The algorithm is applied in the laboratory frame with a separation parameter of 1 and using a P_T weighted recombination scheme [21] in which the jets are treated as massless. The jet algorithm is run on all combined cluster-track objects not previously identified as electron or photon candidates. The scattered electron may fake a jet. This effect is important for multi-jet events, especially at high transverse momenta. To reject these fake jets, the first radial moment of the jet transverse energy [23, 24] is required to be greater than 0.02 and the quantity M^{obj}/P_T^{jet} greater than 0.1 [12,24]. The invariant mass M^{obj} is obtained using the four-vector of all objects belonging to the jet. If the fraction of the jet energy contained in the electromagnetic part of the LAr calorimeter is greater than 0.9, the above criteria are tightened to 0.04 and 0.15, respectively. The jet selection efficiency is 97%.

Neutrino identification A neutrino candidate is defined in events with missing transverse momentum above 20 GeV. The missing momentum is derived from all identified particles and energy deposits in the event. Fake missing transverse momentum may also arise from the mismeasurement of an identified object. This effect is reduced by requiring that the neutrino[3] be isolated from all identified objects with a transverse momentum above 20 GeV. Requiring $\sum_i (E_i - P_{z,i}) < 48$ GeV discards neutrino candidates from NC processes where the missing transverse momentum is caused by energy leakage in the forward region. If exactly one electron or muon object is found, a neutrino object is only assigned to an event if $\Delta\phi(l - X_{tot}) < 170°$, where $\Delta\phi$ is the difference in azimuthal angle between the lepton l and the direction of the system X_{tot} built of all hadronic energies.

Event classification The common phase space for electrons, photons, muons and jets is defined by $10° < \theta < 140°$ and $P_T > 20$ GeV. The neutrino phase space is defined by missing transverse momentum above 20 GeV and $\sum_i (E_i - P_{z,i}) < 48$ GeV. These values are chosen to retain a high selection and trigger efficiency. All particles with $P_T > 20$ GeV, including the neutrino defined by its reconstructed four-vector, are required to be isolated compared with each other by a minimum distance R of one unit in the $\eta - \phi$ plane. The events are classified, depending on the number and types of objects, into exclusive event classes. Events with an isolated calorimetric object in the considered phase space which is not identified as a photon, electron or jet are discarded from the analysis in order to minimise wrong classifications.

Based on these identification criteria purities can be derived for each event class with a sizeable SM expectation. Purity is defined as the ratio of SM events reconstructed in the event class in which they are generated to the total number of reconstructed events in this class. Most purities are found to be above 60% and are close to 100% for the j-j, e-j, j-ν and μ-μ event classes.

3.3 Systematic uncertainties

This section describes the sources of experimental and theoretical systematic uncertainties considered. Experimental systematic uncertainties arising from the measurement of the objects are listed in table 1.

[3] The four-vector of the neutrino is calculated under the assumption $\sum_i (E_i - P_{z,i}) + (E_\nu - P_{z,\nu}) = 55.2$ GeV.

- The electromagnetic energy scale uncertainty varies between 1% and 3% depending on the particle's impact point on the LAr calorimeter surface. The polar angular measurement uncertainty is 3 mrad. The identification of electron and photon candidates depends on the tracking efficiency, which is known with a precision ranging from 3% for polar angles above 37° to 5% in the forward region.

- The hadronic energy scale of the LAr calorimeter is known to 2%. The uncertainty on the jet polar angle determination is 5 mrad for $\theta < 30^\circ$ and 10 mrad for $\theta > 30^\circ$.

- The uncertainty on the transverse momentum measurement for muons is taken to be 5%. The uncertainty on the polar angle is 3 mrad. The muon identification efficiency is known with a precision of 5%.

- The trigger uncertainties for each class are determined by the object with the highest trigger efficiency. The uncertainty on the trigger efficiency is estimated to be 3% if the event is triggered by a jet or missing transverse momentum and 10% if it is triggered by a muon. For electrons and photons the uncertainty on the trigger efficiency is negligible.

- The uncertainty in the integrated luminosity results in an overall normalisation error of 2.5%.

Depending on the dominant production process different theoretical uncertainties are used as listed in table 2. The errors attributed to the predictions for $ep \rightarrow jjX$, $ep \rightarrow j\gamma X$, $ep \rightarrow j\nu X$, $ep \rightarrow jeX$, $ep \rightarrow jj\nu X$, $ep \rightarrow jjeX$ and W production include uncertainties in the parton distribution functions and those due to missing higher order corrections [12, 20, 24, 25]. The error attributed to $ep \rightarrow \mu\mu X$ and $ep \rightarrow eeX$ results mainly from uncertainties in the structure functions [19,26]. The error on the QED Compton cross section is estimated to be 5% for elastic and 10% for inelastic production. An additional theoretical error of 20% is applied for each jet produced by parton shower processes (e.g. 20% for the j-j-j event class). An uncertainty of 50% is added to the prediction for NC DIS events with missing transverse momentum above 20 GeV and a high P_T electron. This uncertainty is estimated by a comparison of the missing transverse momentum distribution between NC DIS events with a low P_T electron ($P_T < 20$ GeV) with the SM prediction.

All systematic errors are added in quadrature and are assigned to the SM predictions.

4 Event yields

All possible event classes with at least two objects are investigated[4]. The event yields subdivided into event classes are presented for the data and SM expectation in figures 1 and 2 for e^+p and e^-p collisions, respectively. All event classes with observed data events or with a SM expectation greater than 1 event are shown. In each class, a good description of the number of observed data events by the SM prediction is seen.

[4]The μ-ν event class is discarded from the present analysis. It is dominated by events in which a poorly reconstructed muon gives rise to missing transverse momentum, which fakes the neutrino signature.

In e^-p collisions, no data events are observed in the event classes μ-j-ν and e-j-ν. Those classes correspond mainly to high P_T W production with a subsequent leptonic decay and the total SM expectation amounts to 1.2 ± 0.2 and 2.5 ± 0.8 in μ-j-ν and e-j-ν classes, respectively. The probability p (see section 4.1) to observe such a downwards fluctuation in the data given the SM expectation is 0.35 and 0.12 in the μ-j-ν and e-j-ν classes, respectively.

5 Search for deviations from the Standard Model

5.1 Search algorithm and strategy

In order to quantify the level of agreement between the data and the SM expectation and to identify regions of possible deviations, the same search algorithm as developed for our previous publication [1] is used. It locates the region of largest deviation of the data from the SM in these distributions.

Definition of regions A region in the $\sum P_T$ and M_{all} distributions is defined as a set of connected histogram bins[5] with a size of at least twice the resolution. All possible regions of any width and at any position in the histograms are considered. The number of data events (N_{obs}), the SM expectation (N_{SM}) and its total systematic uncertainty (δN_{SM}) are calculated for each region.

Probability of a fluctuation of the data in a region A statistical estimator p is defined to judge which region is of most interest. This estimator is derived from the convolution of the Poisson probability density function (pdf) to account for statistical errors with a Gaussian pdf, $G(b; N_{SM}, \delta N_{SM})$, with mean N_{SM} and width δN_{SM}, to include the effect of non negligible systematic uncertainties. The estimator is defined via

$$p = \begin{cases} A \int\limits_0^\infty db\, G(b; N_{SM}, \delta N_{SM}) \sum\limits_{i=N_{obs}}^{\infty} \frac{e^{-b} b^i}{i!} & \text{if } N_{obs} \geq N_{SM} \\ A \int\limits_0^\infty db\, G(b; N_{SM}, \delta N_{SM}) \sum\limits_{i=0}^{N_{obs}} \frac{e^{-b} b^i}{i!} & \text{if } N_{obs} < N_{SM} \end{cases}$$

$$\text{with} \quad A = 1 / \left[\int\limits_0^\infty db\, G(b; N_{SM}, \delta N_{SM}) \sum_{i=0}^{\infty} \frac{e^{-b} b^i}{i!} \right].$$

The factor A ensures normalisation to unity. If G is replaced by a Dirac delta function $\delta(b - N_{SM})$ the estimator p becomes the usual Poisson probability. The value of p gives an estimate of the probability of a fluctuation of the SM expectation upwards (downwards) to at least (at most) the observed number of data events in the region considered.

[5] In order to minimise binning effects, a bin size smaller than the resolution of the researched quantity is used. All values presented in this study are derived using a 5 GeV bin size for all distributions. Further reduction of the bin size has a negligible effect on the results.

Determination of the most interesting region A possible sign of new physics is found if the expectation significantly disagrees with the data. A disagreement is quantified by the estimator p. The region of greatest interest (of greatest deviation) is the region having the smallest p-value, p_{min}.

Significance per event class The possibility that a fluctuation with a value p_{min} occurs anywhere in the distribution is estimated using the following method. Many independent hypothetical data histograms are made by filling each bin with an event number diced according to the pdfs of the SM expectation (again a convolution of Poisson and Gaussian pdfs). For each of those hypothetical data histograms the algorithm is run to find the region of greatest deviation and the corresponding p^{SM}_{min} is calculated. The probability $\hat{P}$ is then defined as the fraction of hypothetical data histograms with a p^{SM}_{min} equal to or smaller than the p_{min} value obtained from the real data. The $\hat{P}$ values of event classes with no data event and a SM expectation $\lesssim 1$ are 1. $\hat{P}$ is a measure of the statistical significance of the deviation observed in the data. If the event classes are exclusive, $\hat{P}$ can be used to compare results of different event classes. Consequently the event class of most interest for a search is the one with the smallest $\hat{P}$ value. Depending on the final state, a p_{min}-value of $5.7 \cdot 10^{-7}$ ("5σ") corresponds to a value of $-\log_{10} \hat{P}$, the negative decade logarithm of $\hat{P}$, between 5 and 6.

Global significance The overall degree of agreement with the SM can further be quantified by taking into account the large number of event classes studied in this analysis. Among all studied classes there is some chance that small $\hat{P}$ values occur. This probability can be calculated with MC experiments. A MC experiment is defined as a set of hypothetical data histograms (either in M_{all} or in $\sum P_T$) following the SM expectation with an integrated luminosity equal to the amount of data recorded.

The complete search algorithm and statistical analysis are applied to the MC experiments like for data. This procedure is repeated many times. The expectation for the $\hat{P}$ values observed in the data is then given by the distribution of $\hat{P}^{SM}$ values obtained from all MC experiments. The probability to find in MC experiments a $\hat{P}$ value smaller than in the data can be calculated and gives us the global significance of the observed deviation.

5.2 Search results

The $\hat{P}$ values observed in the real data in all event classes are compared in figures 3 and 4 to the distribution of $\hat{P}^{SM}$ obtained from the large set of MC experiments, normalised to one experiment. The comparison is presented for the scans of the invariant mass distributions and $\sum P_T$ distributions. All $\hat{P}$ values range from 0.01 to 0.99, corresponding to event classes where no significant discrepancy between data and the SM expectation is observed. These results are in agreement with the expectation from MC experiments.

The regions selected by the algorithm in $\sum P_T$ and M_{all} distributions of each class are presented for e^+p data in figures 5 and 6, respectively. The distributions of $\sum P_T$ and M_{all} observed in e^-p data are displayed in figures 7 and 8, respectively.

Due to the uncertainties of the SM prediction in the j-j-j-j and j-j-j-j-ν event classes at highest M_{all} and $\sum P_T$ (see [1]), where data events are observed, no reliable $\hat{P}$ values can be calculated for these classes. These event classes are not considered to search for deviations from the SM in this extreme kinematic domain. Consequently, these event classes are not taken into account to determine the overall degree of agreement between the data and the SM.

The most significant deviation from SM predictions is observed in the μ-j-ν event class and in e^+p collisions with a value of $-\log_{10}\hat{P}$ equal to 1.7. In our previous analysis [1] based on HERA I data dominated by e^+p collisions, the largest deviation was also found in this event class, with $-\log_{10}\hat{P} = 3$.

6 Summary

All the data collected with the H1 experiment during HERA II running period (2003–2007) have been investigated for deviations from the SM prediction at high transverse momentum. All event topologies involving isolated electrons, photons, muons, neutrinos and jets are investigated in a single analysis. A good agreement between data and SM expectation is found in most event classes. In each event class the invariant mass and sum of transverse momenta distributions of particles have been systematically searched for deviations using a statistical algorithm. No very significant deviation is observed in the phase-space and in the event topologies covered by this analysis. The largest deviation from SM expectation is observed in the μ-j-ν event class in e^+p collisions.

References

[1] A. Aktas *et al.* [H1 Collaboration], Phys. Lett. B **602** (2004) 14 [arXiv:hep-ex/0408044].

[2] R. Brun, F. Bruyant, M. Maire, A. C. McPherson and P. Zanarini, CERN-DD/EE/84-1.

[3] T. Sjostrand, P. Eden, C. Friberg, L. Lonnblad, G. Miu, S. Mrenna and E. Norrbin, Comput. Phys. Commun. **135** (2001) 238 [hep-ph/0010017].

[4] H. Jung, Comput. Phys. Commun. **86** (1995) 147.

[5] A. Kwiatkowski, H. Spiesberger and H. J. Mohring, Comput. Phys. Commun. **69** (1992) 155.

[6] C. Berger and P. Kandel, Prepared for Workshop on Monte Carlo Generators for HERA Physics Hamburg, Germany, 27-30 Apr 1998.

[7] T. Abe, Comput. Phys. Commun. **136** (2001) 126 [hep-ph/0012029].

[8] A. Mucke, R. Engel, J. P. Rachen, R. J. Protheroe and T. Stanev, Comput. Phys. Commun. **124** (2000) 290 [astro-ph/9903478].

[9] U. Baur, J. A. Vermaseren and D. Zeppenfeld, Nucl. Phys. B **375** (1992) 3.

[10] K. P. Diener, C. Schwanenberger and M. Spira, Eur. Phys. J. C **25** (2002) 405 [arXiv:hep-ph/0203269].

[11] K. P. Diener, C. Schwanenberger and M. Spira, [hep-ex/0302040].

[12] C. Adloff *et al.* [H1 Collaboration], Eur. Phys. J. C **25** (2002) 13 [hep-ex/0201006].

[13] I. Abt *et al.* [H1 Collaboration], Nucl. Instrum. Meth. A **386** (1997) 310.

[14] I. Abt *et al.* [H1 Collaboration], Nucl. Instrum. Meth. A **386** (1997) 348.

[15] B. Andrieu *et al.* [H1 Calorimeter Group Collaboration], Nucl. Instrum. Meth. A **336** (1993) 460.

[16] R. D. Appuhn *et al.* [H1 SPACAL Group Collaboration], Nucl. Instrum. Meth. A **386** (1997) 397.

[17] C. Adloff *et al.* [H1 Collaboration], Eur. Phys. J. C **30**, 1 (2003) [hep-ex/0304003].

[18] M. Peez, "Recherche de déviations au Model Standard dans les processus de grande énergie transverse sur le collisionneur électron - proton HERA", Ph.D. thesis, Université de Lyon (2003), DESY-THESIS-2003-023. (available at http://www-h1.desy.de/psfiles/theses/).

[19] A. Aktas *et al.* [H1 Collaboration], Phys. Lett. B **583** (2004) 28 [hep-ex/0311015].

[20] V. Andreev *et al.* [H1 Collaboration], Phys. Lett. B **561** (2003) 241 [hep-ex/0301030].

[21] S. D. Ellis and D. E. Soper, Phys. Rev. D **48** (1993) 3160 [hep-ph/9305266].

[22] S. Catani, Y. L. Dokshitzer, M. H. Seymour and B. R. Webber, Nucl. Phys. B **406** (1993) 187.

[23] W. T. Giele, E. W. N. Glover and D. A. Kosower, Phys. Rev. D **57** (1998) 1878 [arXiv:hep-ph/9706210].

[24] G. Frising, "Rare Phenomena and W production in Electron-Proton Scattering at HERA", Ph.D. thesis, RWTH Aachen (2003) (available at http://www-h1.desy.de/psfiles/theses/).

[25] M. Wessels, "General Search for New Phenomena in ep Scattering at HERA", Ph.D. thesis, RWTH Aachen (2004) (available at http://www-h1.desy.de/psfiles/theses/).

[26] A. Aktas *et al.* [H1 Collaboration], Eur. Phys. J. C **31** (2003) 17 [hep-ex/0307015].

Object	Energy Scale	θ (mrad)	Identification efficiency
Jet	2%	5–10	–
Electron	1–3%	1–3	3–5%
Photon	1–3%	1–3	5–15%
Muon	5%	3	5%

Table 1: Systematic uncertainties attributed to the measurement of energies, polar angles and to the identification efficiencies of particles.

Process	Uncertainty
$ep \to jjX$ and $ep \to j\gamma X$	15%
$ep \to j\nu X$ and $ep \to jeX$	10%
$ep \to jj\nu X$ and $ep \to jjeX$	15%
$ep \to \mu\mu X$ and $ep \to eeX$	3%
$ep \to WX$ and $ep \to WjX$	15%
$ep \to e\gamma X$ and $ep \to e\gamma j$	10%
$ep \to e\gamma p$	5%

Table 2: Theoretical uncertainties attributed to the simulation of different SM processes.

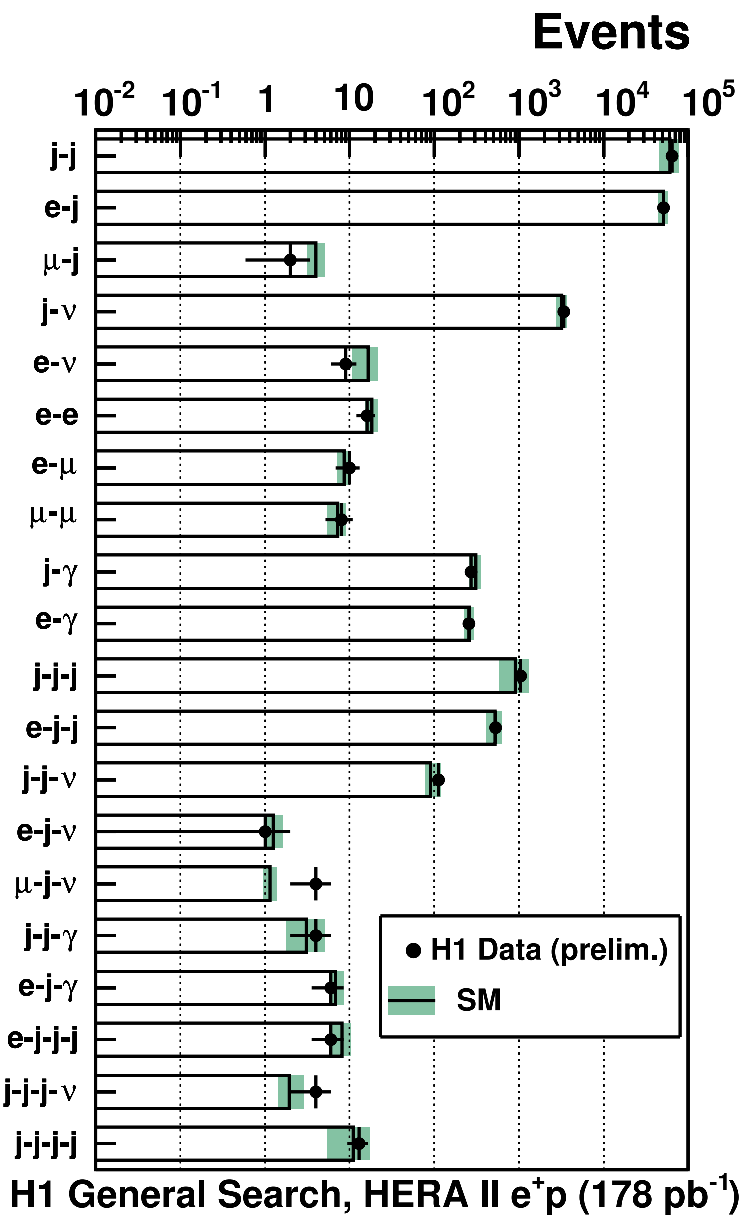

Figure 1: The data and the SM expectation for all event classes with observed data events or a SM expectation greater than 1 events. The analysed data sample corresponds to an integrated luminosity of 178 pb^{-1} recorded in $e^{+}p$ collisions. The error bands on the predictions include model uncertainties and experimental systematic errors added in quadrature.

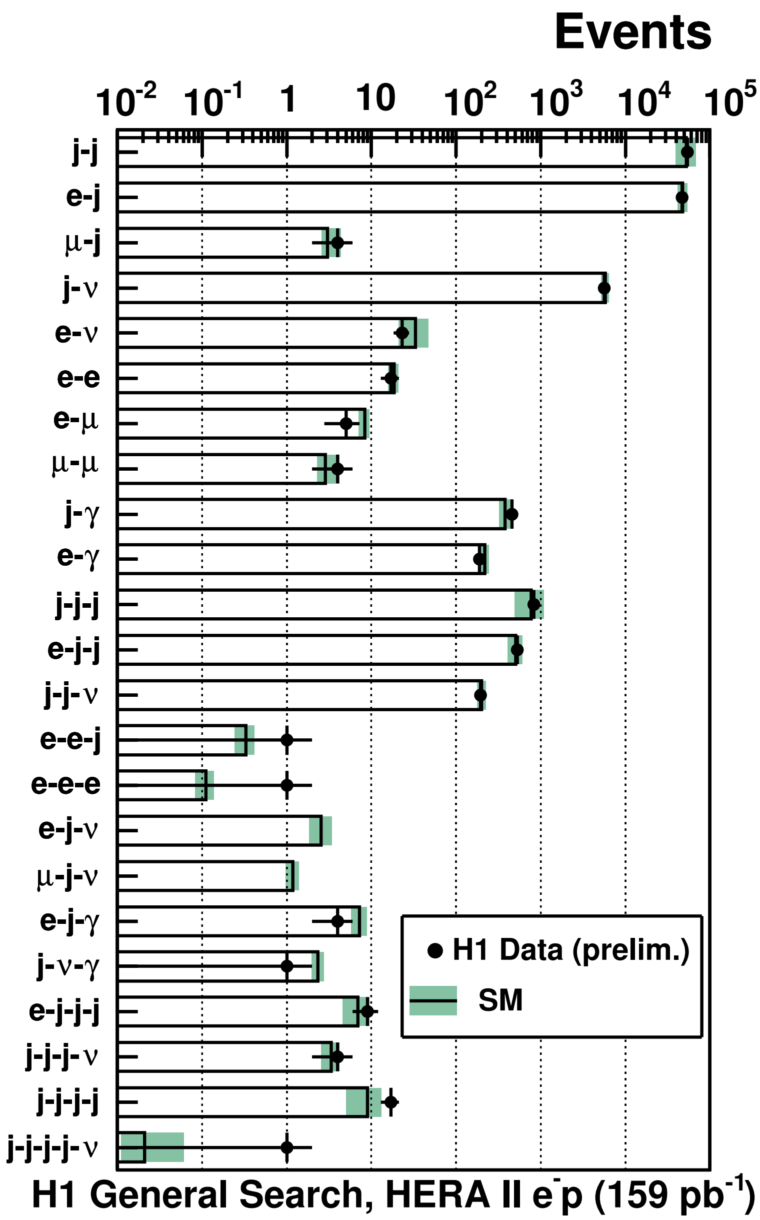

Figure 2: The data and the SM expectation for all event classes with observed data events or a SM expectation greater than 1 events. The analysed data sample corresponds to an integrated luminosity of 159 pb^{-1} recorded in e^-p collisions. The error bands on the predictions include model uncertainties and experimental systematic errors added in quadrature.

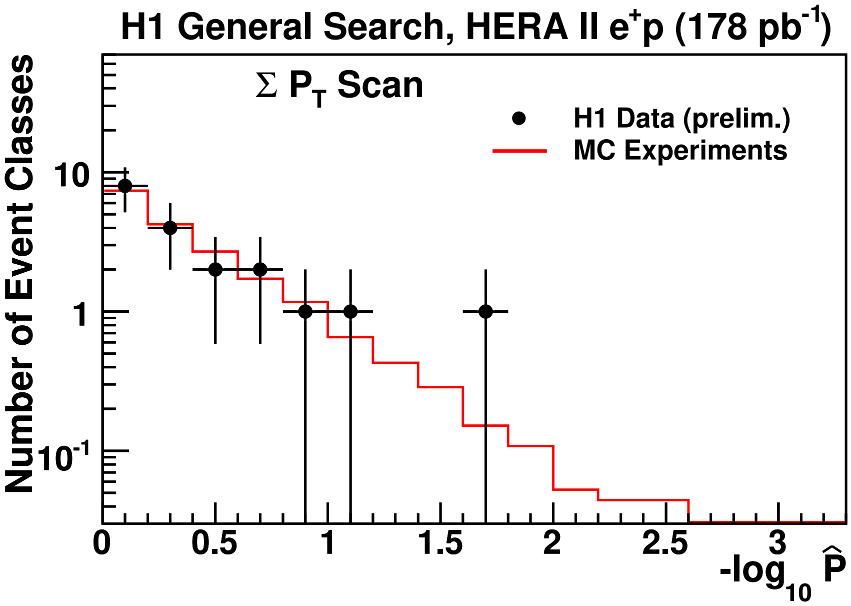

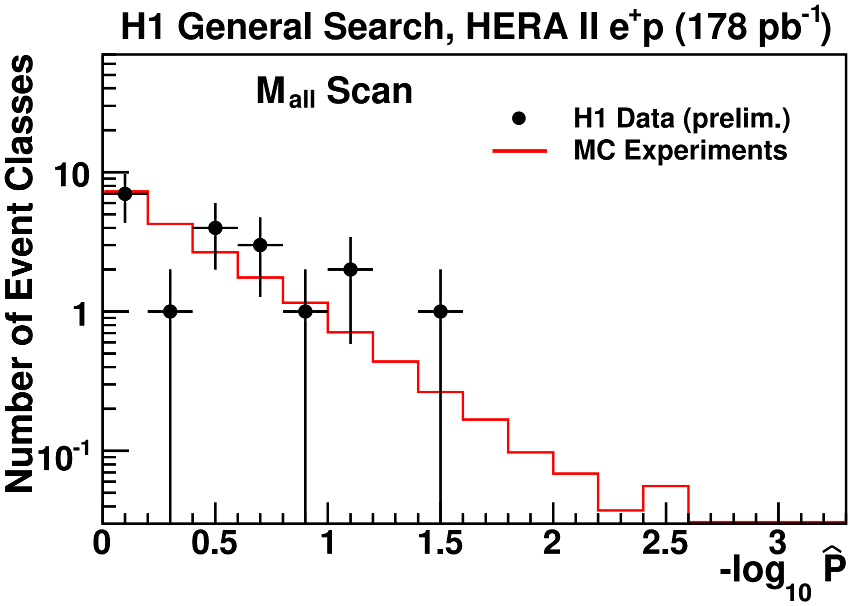

Figure 3: The $-\log_{10}\hat{P}$ values for the data event classes and the expected distribution from MC experiments as derived by investigating the $\sum P_T$ distributions (top) and $M_{\rm all}$ distributions (bottom) with the search algorithm. The analysed data sample corresponds to an integrated luminosity of 178 pb^{-1} recorded in e^+p collisions.

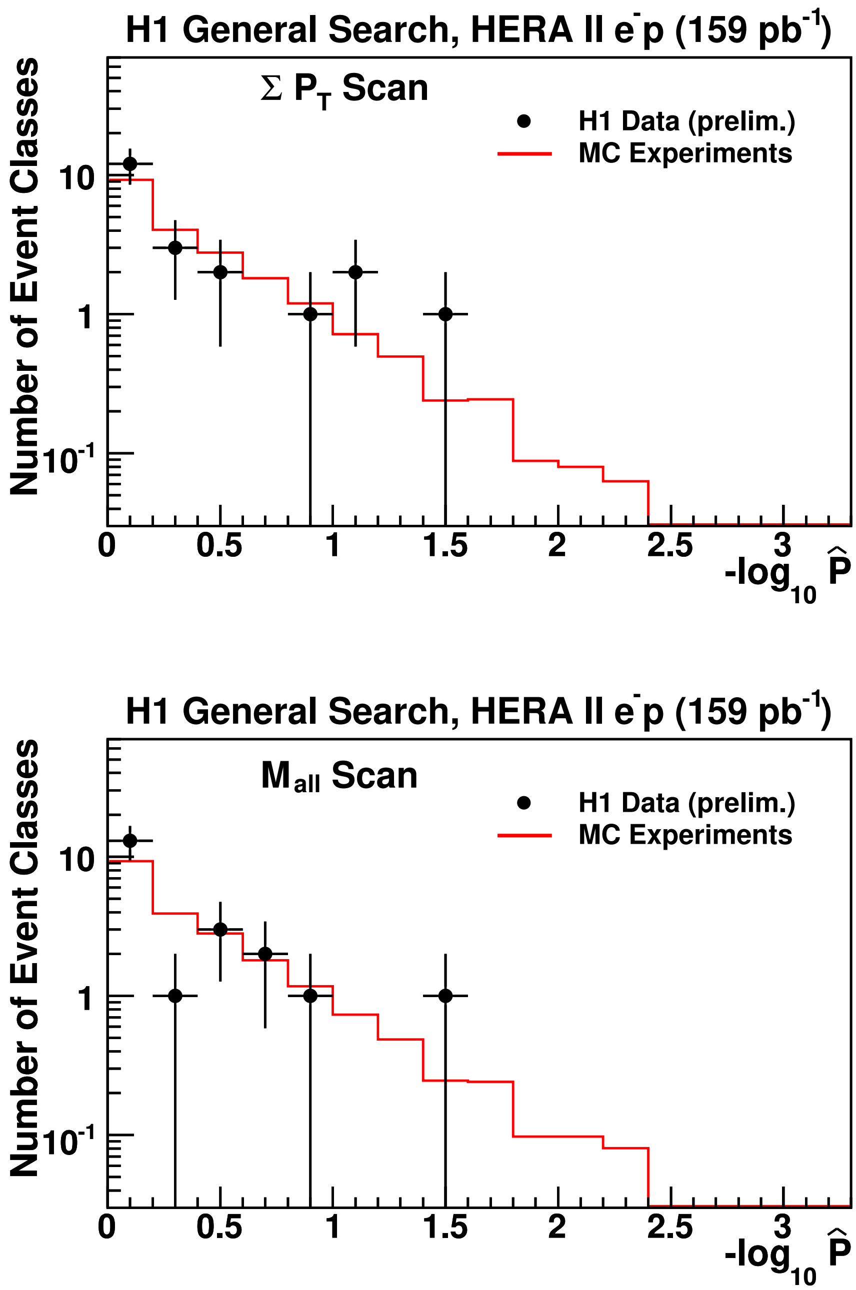

Figure 4: The $-\log_{10}\hat{P}$ values for the data event classes and the expected distribution from MC experiments as derived by investigating the $\sum P_T$ distributions (top) and $M_{\rm all}$ distributions (bottom) with the search algorithm. The analysed data sample corresponds to an integrated luminosity of 159 pb^{-1} recorded in e^-p collisions.

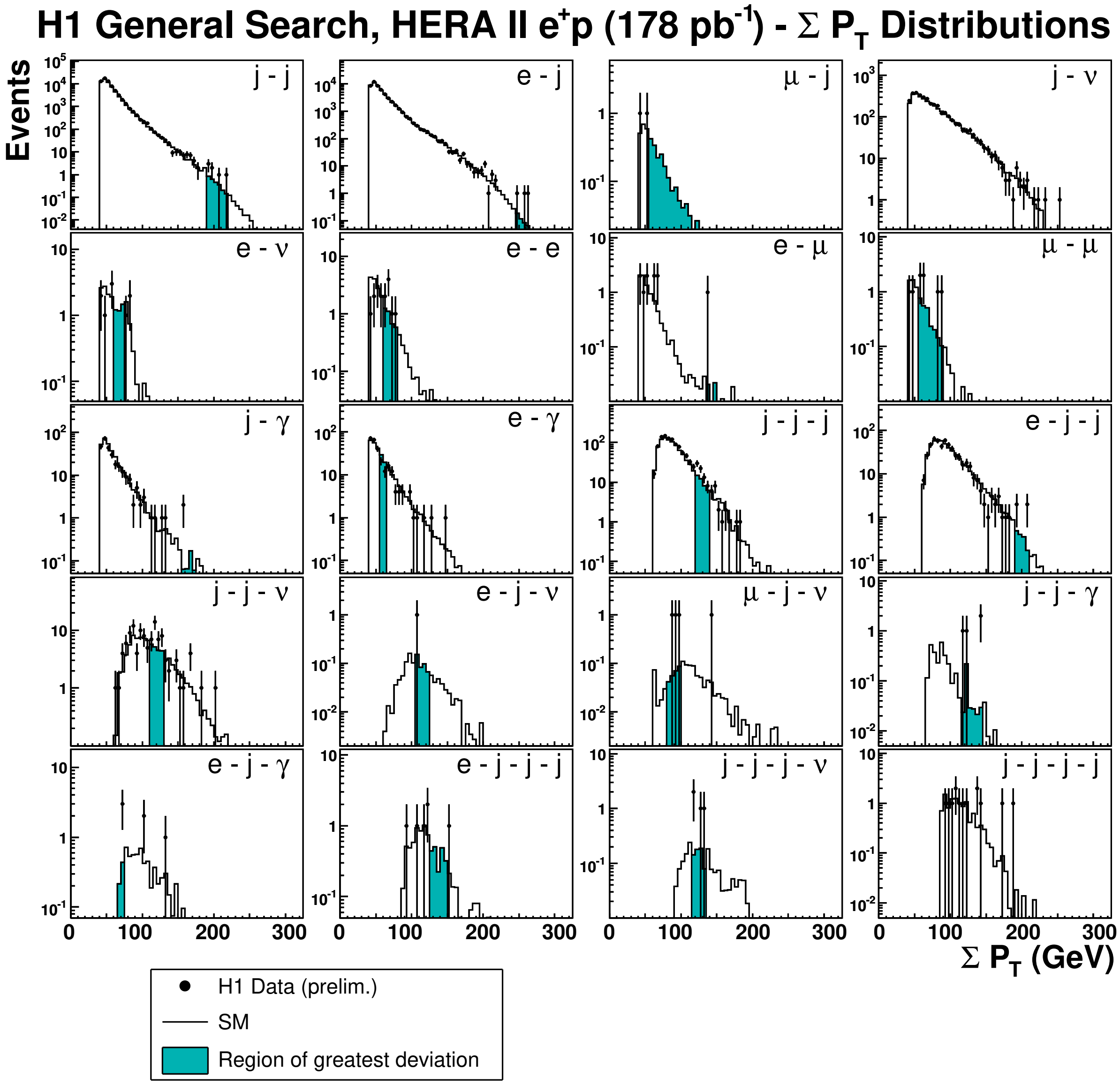

Figure 5: The number of data events and the SM expectation as a function of $\sum P_T$ for classes with at least one event, for e^+p HERA II data. The shaded areas show the regions of greatest deviation chosen by the search algorithm. No search is performed for the j-j-j-j class.

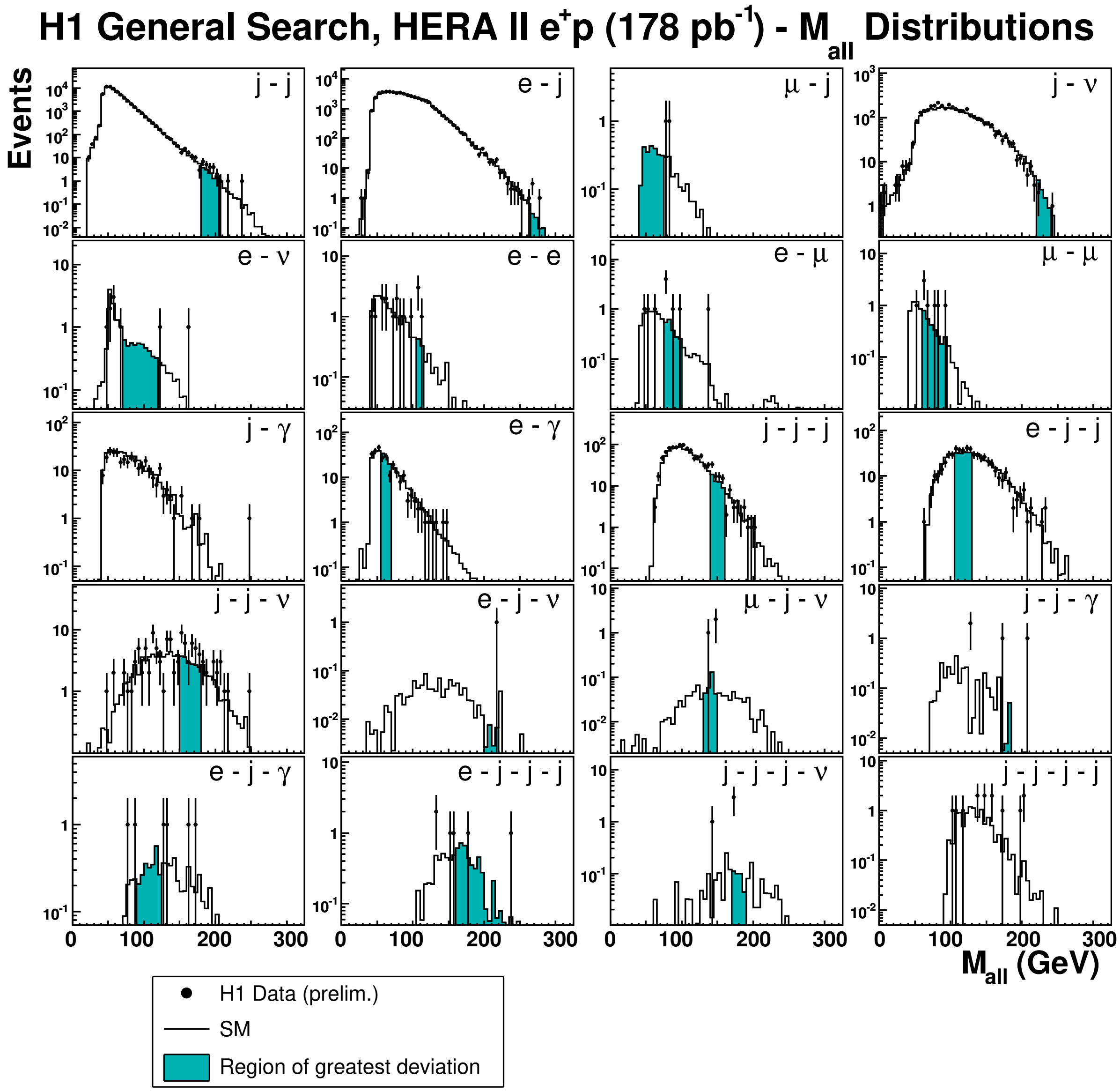

Figure 6: The number of data events and the SM expectation as a function of $M_{\rm all}$ for event classes with at least one event, for e^+p HERA II data. The shaded areas show the regions of greatest deviation chosen by the search algorithm. No search is performed for the j-j-j-j class.

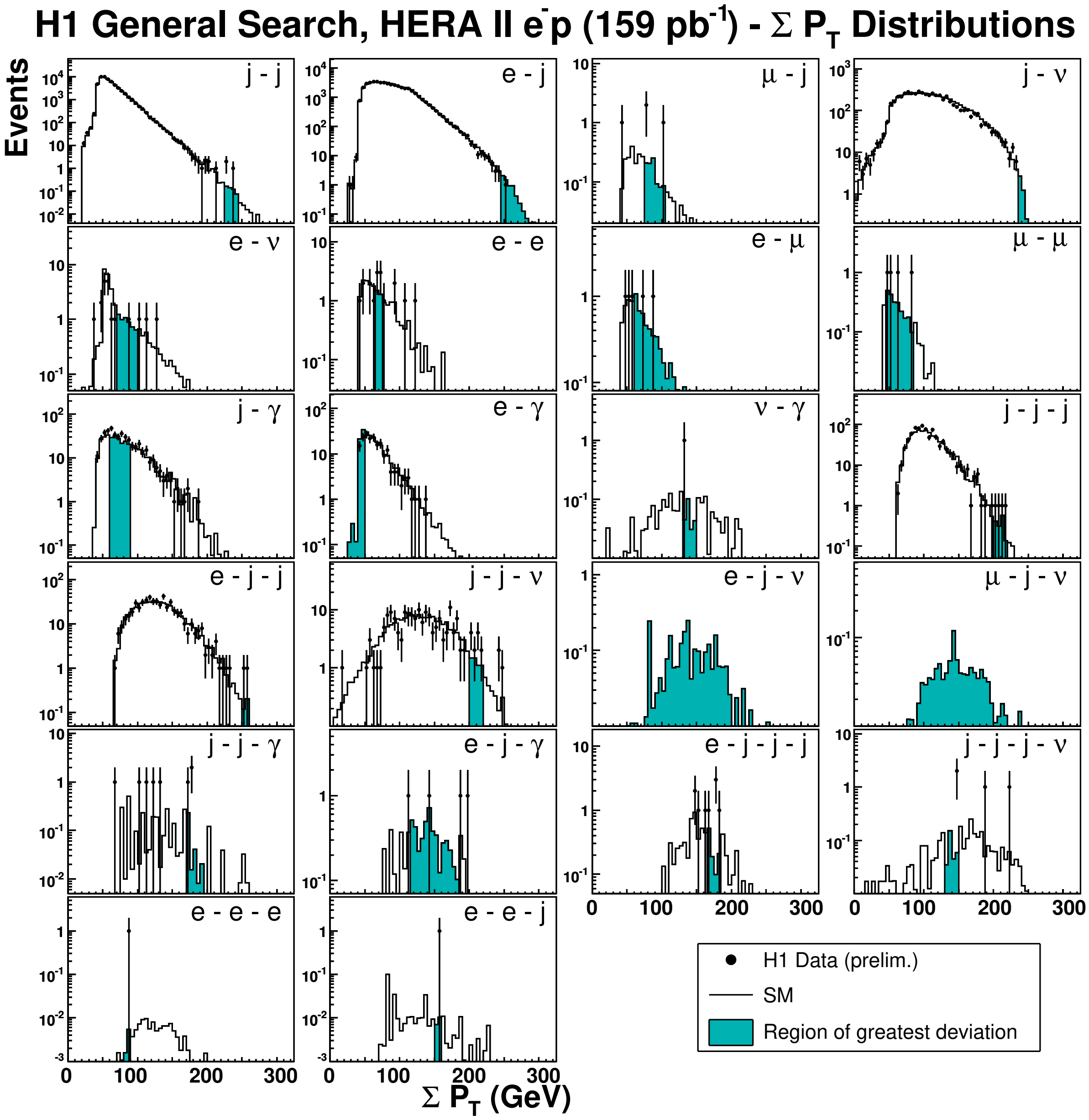

Figure 7: The number of data events and the SM expectation as a function of $\sum P_T$ for classes with at least one event, for e^-p HERA II data. The shaded areas show the regions of greatest deviation chosen by the search algorithm. No search is performed for the j-j-j-j and j-j-j-j-ν classes.

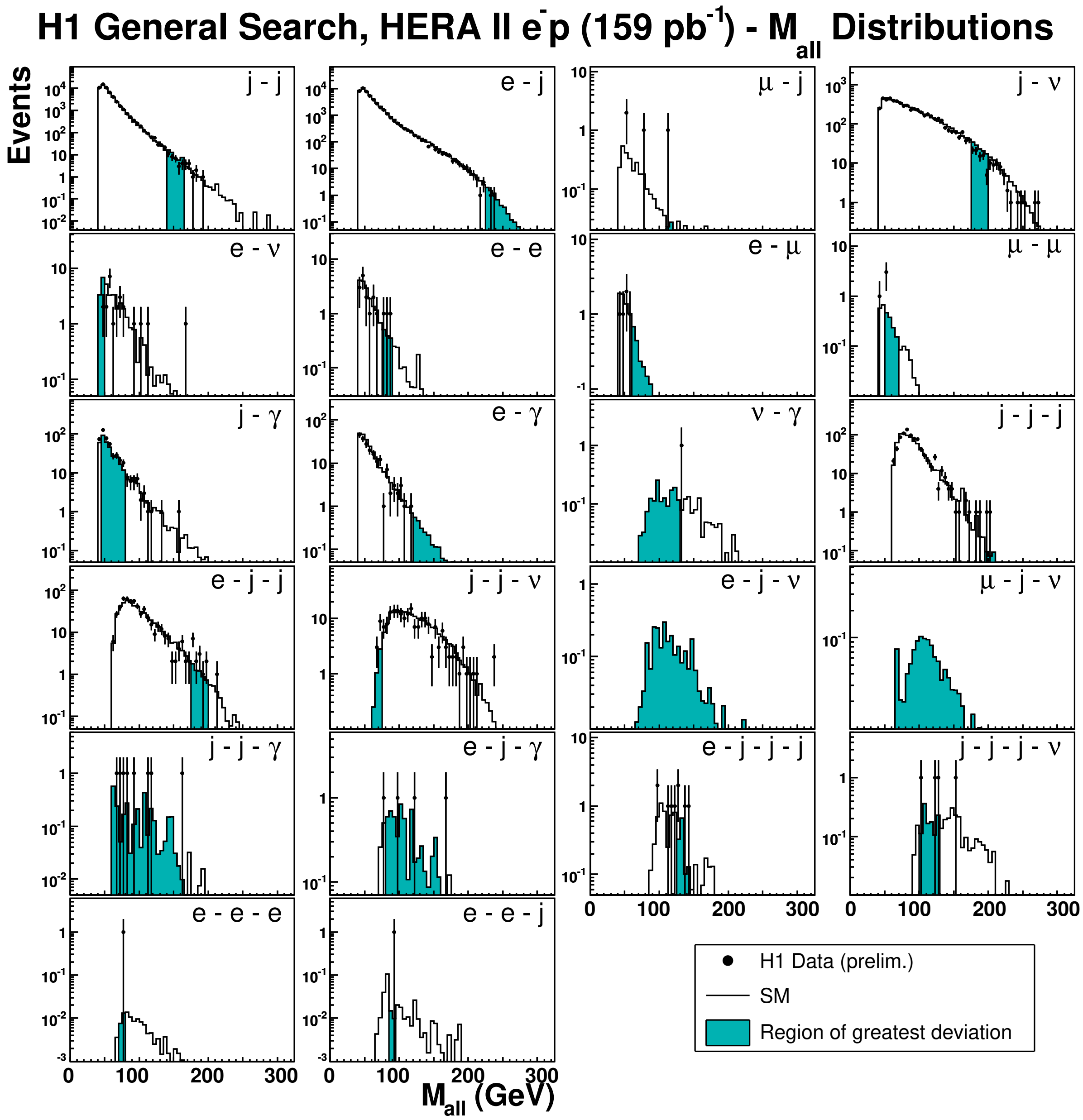

Figure 8: The number of data events and the SM expectation as a function of M_{all} for event classes with at least one event, for $e^{-}p$ HERA II data. The shaded areas show the regions of greatest deviation chosen by the search algorithm. No search is performed for the j-j-j-j and j-j-j-j-ν classes.